Intensity–Duration–Frequency curves of precipitation at the global scale

Laurent G. Courty[a,*], Robert L. Wilby[a], John K. Hillier[a], Louise J. Slater[b]

[a]*Department of Geography and Environment, Loughborough University, LE11 3TU, UK*
[b]*School of Geography and Environment, University of Oxford, OX1 3QY, UK*

Abstract

Intensity-Duration-Frequency (IDF) curves usefully quantify extreme precipitation. Unfortunately, sparse, infrequent or short observations hinder the creation of robust IDF curves in many locations around the world. This paper presents a global, multi-temporal (1 h to 360 h) dataset of Gumbel parameters at 30 km resolution dubbed PXR-2 (Parametrized eXtreme Rain). Using these data we show that the two Gumbel parameters typically scale robustly with event duration ($r^2 > 0.85$, $p < 0.01$). Thus, we propose a four-parameter IDF formula that allows estimates of rainfall intensity for a continuous range of durations (PXR-4). This parameter scaling property opens the door to estimating sub-daily IDF from daily records. We evaluate this characteristic for selected global cities and a rain gauge network in the United Kingdom. PXR aims to be of immediate use for engineers for designing critical infrastructure such as urban drainage systems, dams and highways, with potential applications in other fields of earth sciences.

Keywords: Frequency analysis, precipitation, design rainfall, ERA5, reanalysis

---

*Corresponding author
Email address: `l.courty@lboro.ac.uk` (Laurent G. Courty)

1. Introduction

Historical precipitation records are widely employed by civil engineers to compute Intensity–Duration–Frequency (IDF) curves, which are essential for the design of infrastructure like highways (e.g. Brown et al., 2013; NYS DoT, 2018), urban drainage networks (e.g. Battaglia et al., 2003; Brown et al., 2013) and dams (e.g. NYS DoEC, 1989). Indeed, IDF curves are used to create synthetic rainfalls that permit the sizing of a structure for a given return period, often required by local regulations.

However, not all countries have historical rain gauge records that are long or dense enough to compute reliable IDF curves (e.g. Lumbroso et al., 2011). The lack of observational data for IDF analysis is particularly true in continents such as Africa (van de Giesen et al., 2014) and Asia, where most of the world's urbanization is expected to take place in the coming decades (UN DESA, 2018). As a result, much new infrastructure is being built in regions where the historical record of rainfall is scarce or uncertain, hindering adequate sizing of water-related works.

The first limitation of the observational data records is the scarcity of spatial coverage. The classical approach to circumvent this aspect of data scarcity is to interpolate rainfall between weather stations. However this approach is unlikely to perform well when pluviometers are sparse (e.g. Xu et al., 2015; Kumari et al., 2017). One approach recognized as more advanced consists of analyzing regional precipitation patterns to estimate local characteristics such as IDF curves at the location of interest (e.g. Roux and Desbordes, 1996; Fowler and Kilsby, 2003; Domínguez et al., 2018). Most recently, IDF curves have been derived over the continental U.S. (Ombadi et al., 2018) using the PERSIANN-CDR satellite-based precipitation dataset (Ashouri et al., 2015). But to the best of our knowledge a global, consistent IDF dataset is still lacking.

Thus, the increasing resolution and reliability of global or near-global gridded precipitation datasets represents a key opportunity to develop alternative approaches to tackle engineering challenges such as the correct sizing of flood infrastructure. Global gridded precipitation estimates are typically obtained by meteorological reanalysis (e.g. Gelaro et al., 2017; Uppala et al., 2005), whereby weather observations have been assimilated by numerical weather prediction models. Alternatively, recent schemes have also been obtained by merging gauge-, satellite-, and reanalysis-based data to generate enhanced global precipitation estimates (e.g. Beck et al., 2018; Sun et al., 2018). Although global weather data products are widely employed by the earth science community, their use in engineering is still limited to applications such as wind power generation (e.g. Staffell and Pfenninger, 2016; Olauson, 2018) or drought monitoring (e.g. Hao et al., 2014). As far as we are aware, this paper is the first attempt to study global IDF relationships using gridded precipitation datasets, an effort that could help solving the issue of precipitation data scarcity.

A second issue that is common with precipitation data is temporal resolution. In many cases, sub-daily IDF records are required for engineering uses because small catchments that are sensitive to brief rainfall events often require appropriate storm-water drainage structures. However, the vast majority of historical precipitation data are still collected at a daily resolution. Specifically, such low temporal resolution presents a challenge for engineers tasked with the design of urban water infrastructure, where catchments are commonly a few hectares with lag times less than an hour (Berne et al., 2004).

This limitation could be mitigated by using a temporal scaling property of IDF curves to estimate sub-daily IDF from daily precipitation. Extreme precipitation intensities for a given event duration d typically follow a Generalized Extreme Value (GEV) distribution, and it has been shown that the location and scale parameters of the GEV scale with d (e.g. Menabde et al., 1999; Bougadis and Adamows, 2006; Overeem et al., 2008; Veneziano and Furcolo, 2002). For instance, Menabde et al. (1999) argued that the IDF characteristic of a given site could be described by a Gumbel distribution whose parameters follow a power law for durations between 30 min and 24 h. However, those studies analyzed only a few sites—e.g. 2 in South Africa and Australia in Menabde et al. (1999), 5 in Canada in Bougadis and Adamows (2006), 12 in the Netherlands in

Overeem et al. (2008)—and did not assess whether or not this scaling property holds at a global scale. Understanding to what extent sub-daily IDF can be estimated from daily precipitation data is of practical interest in many parts of the world where daily rainfall data are more widely available than sub-daily records.

This paper firstly uses the ERA5 reanalysis to generate global IDF relationships modelled with a Gumbel distribution, then investigates if these relationships scale with the event duration d at a global level. Finally, we assess the extent to which this scaling property can be used to estimate sub-daily rainfall patterns using daily data. This work results in the creation of two datasets. The Parameterized eXtreme Rainfall–2 (PXR-2) compiles the Gumbel parameters for 19 events durations, whereas the Parameterized eXtreme Rainfall–4 (PXR-4) represents the global distribution of the four parameters of a generalized IDF formula. Fully describing or explaining the rich detail of the PXR dataset is beyond the scope of this paper.

2. Methodology

2.1. Input data

Precipitation data are from the ERA5 deterministic reanalysis (Hersbach and Dick, 2016; Copernicus Climate Change Service, 2018), with a spatial resolution of 0.25° (∼30 km) and temporal resolution of 1 h. We chose the ERA5 dataset for its high spatial and temporal resolution, and its performance (Beck et al., 2018). We employ all the complete calendar years available at the time of writing (i.e. 2000-2017). Whilst 18 years is a relatively short time scale, the same analysis could be performed with a longer dataset once it becomes available.

As a reference, and for comparison with the reanalysis data, we use hourly rain gauge records from the MIDAS database of the UK Meteorological Office (Met Office, 2012). The original dataset contains 682 stations with variable record lengths. Following Blenkinsop et al. (2017), we keep only the observations that do not exceed by more than 20 % the 1 h and 24 h precipitation historical maxima for the UK, measured as 92 mm and 279 mm by Met Office (2018). After this quality control, we flag the years with $\geq$ 90 % of remaining observations, and then keep only stations that fulfill this criterion for $\geq$ 90 % of those years (i.e. 16 of 18). 97 stations remain (see Fig. S1).

2.2. Global Gumbel parameters scaling

Annual maxima of precipitation are assumed to follow a Gumbel distribution with the Cumulative Distribution Function (CDF) (1), where i is the rainfall intensity, μ the location parameter and σ the scale parameter. This assumption is supported by computing the Anderson-Darling A^2. According to this test, the null hypothesis that the annual maxima follow a Gumbel distribution can be rejected for only 4.6 % of the cells at the 1 % significance level. The null hypothesis rejection occurs mostly above oceans and in desert regions (see Figure S2).

$$F(i; \mu, \sigma) = e^{-e^{-z}} \tag{1a}$$

$$z = \frac{i - \mu}{\sigma} \tag{1b}$$

To assess the scaling of the distribution parameters relative to the event duration, we find the annual maxima for a series of 19 event durations d by using a rolling mean. The window sizes are chosen to reflect a relatively regular spacing on a logarithmic scale and to present an equal number of durations for sub- and super-daily events. The selected sub- and super-daily durations are 1, 2, 3, 4, 6, 8, 10, 12, 18 and 24 h and 1, 2, 3, 4, 5, 6, 8, 10, 12 and 15 days, respectively. Then, for each duration and ERA5 cell, the Gumbel distribution's location μ and scale σ parameters are obtained by the maximum likelihood method (i.e. SciPy, Jones et al., 2001). The global maps of those parameters for each duration are compiled in the PXR-2 dataset (Courty et al., 2018).

Following Menabde et al. (1999), we assume that μ and σ scale with d according to a power law, but where they assert a single scaling gradient for both parameters we allow each to scale independently. This independent scaling of the two parameters appears typical for ERA5 data (Fig. S3 and S4). The scaling is therefore expressed as

$$\mu_d = ad^{\alpha} \tag{2a}$$

$$\sigma_d = bd^{\beta} \tag{2b}$$

where d is the duration and α, β , a and b are the scaling parameters. These power-law relationships are straight lines in logarithmic space as shown by (3). For simplicity and ease of reproducibility (e.g. by practitioners) the scaling parameters are then estimated by Ordinary Least Squares (OLS) regression. The existence and prevalence of power law scaling can then be assessed by calculating the Pearson's r correlation coefficient on the log-transformed data. The PXR-4 dataset (Courty et al., 2018) comprises the global distribution of these four parameters.

$$\log_{10}(\mu_d) = \alpha \log_{10}(d) + log_{10}(a) \tag{3a}$$

$$\log_{10}(\sigma_d) = \beta \log_{10}(d) + log_{10}(b) \tag{3b}$$

2.3. Estimation of sub-daily parameters using daily data

To quantify how well sub-daily IDF parameters can be estimated from daily precipitation records, we fit an OLS regression line on the Gumbel parameters as in Section 2.2, but using only durations of 24 h and above. Then, in logarithmic space, the sub-daily prediction can be compared to observations from ERA5 and MIDAS.

3. Results

3.1. Global Gumbel parameters

The PXR-2 dataset comprises worldwide Gumbel parameters estimated from the ERA data for all 19 durations (1 h to 360 h). This dataset is made freely available to accompany this paper (Courty et al., 2018). The Gumbel parameter maps for an event duration of 24 hours in Fig. 1 clearly display regional rainfall patterns, such as tropical rainfall and monsoon (e.g. south Asia, Kripalani et al., 2007), orographic rainfall over mountainous regions (e.g. central Andes, Viale et al., 2011), and desert areas (e.g. Antartica, Vaughan et al., 1999).

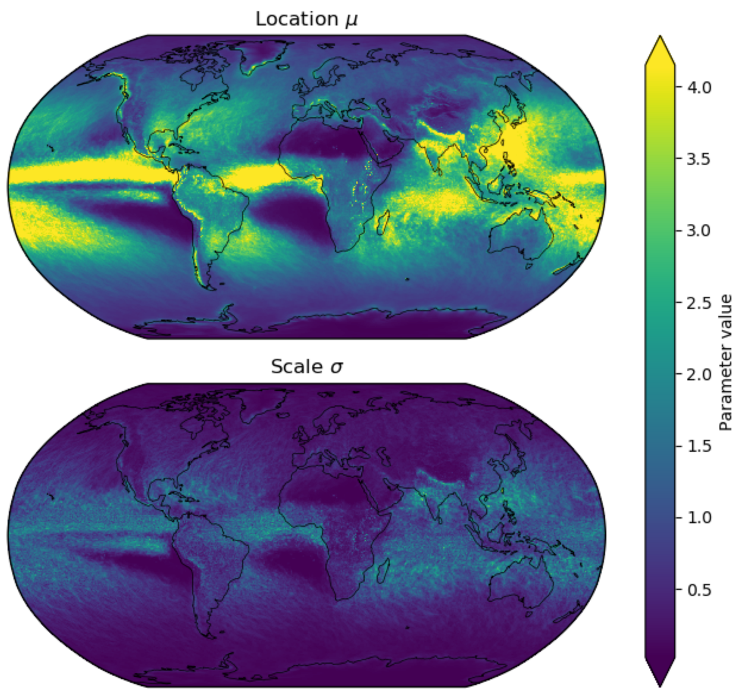

Figure 1: Global distribution of the Gumbel parameter values for an event duration of 24 h. The values for event durations from 1 h to 360 h are available in the PXR-2 dataset (Courty et al., 2018).

3.2. Scaling of the Gumbel parameters

The fit of the relationship between μ or σ and d is quantified by calculating Pearson's coefficient of determination (i.e. r^2) for data presented on a log-log scale. In 99 % of the ERA cells r^2 exceeds 0.91 for μ and 0.85 for σ. In other words, both the logarithms of parameters have strong linear relationships with the logarithm of duration, although these relationships are stronger for the location than scale. Furthermore, in all but 0.02 % of cells the relationship is highly significant (i.e. $p < 0.01$). Thus, the Gumbel parameters scale linearly and this property appears to be robust and consistent at the global scale. A tabulation of further r^2 thresholds and global map of r^2 values are given in supplementary material (see Table S1 and Fig. S5).

Fig. 2 illustrates how this scaling applies for selected global cities. The goodness of fit varies depending on the city, and the fitted regression lines tend to overestimate both Gumbel parameters at shorter durations (more on this in Section 3.3.) Additionally, the scale parameter σ displays a weaker linear scaling, a property that is in accordance with the r^2 values.

3.3. Estimation of sub-daily parameters using daily data

Following the observation that the global ERA Gumbel parameters μ and σ scale consistently with d (Section 3.2) it is pertinent to quantify the predictability of sub-daily parameters when only daily rainfall data are available. Fig. 3 compares the differences in scaling slope when (i) using all the durations from hourly to multi-daily, and (ii) using only super-daily durations. Overall, a preponderance of ratios <1 indicate that any tendency to an apparent overestimation of both Gumbel parameters at shorter durations (i.e. <24 h) is exacerbated when the regression line is fitted to super-daily durations. For μ, a geographical pattern is noticeable, where the use of daily data induces an apparent overestimation at shorter d across most of the globe, but an apparent underestimation of μ in much of sub-Saharan Africa, South-East Asia and the Tibetan Plateau, and in the region from Mexico to northern half of South America. Similarly, Antarctica and Greenland display large apparent overestimations when using the daily data for estimating sub-daily parameters. Conversely, the scale parameter σ does not display a strong large-scale geographical pattern, and indicates widespread apparent overestimation of σ at short durations, but with stronger local variations. This relatively small-scale variability is consistent with the greater sensitivity of σ (i.e. less robustly constrained) than μ (see Fig. 1 and 2).

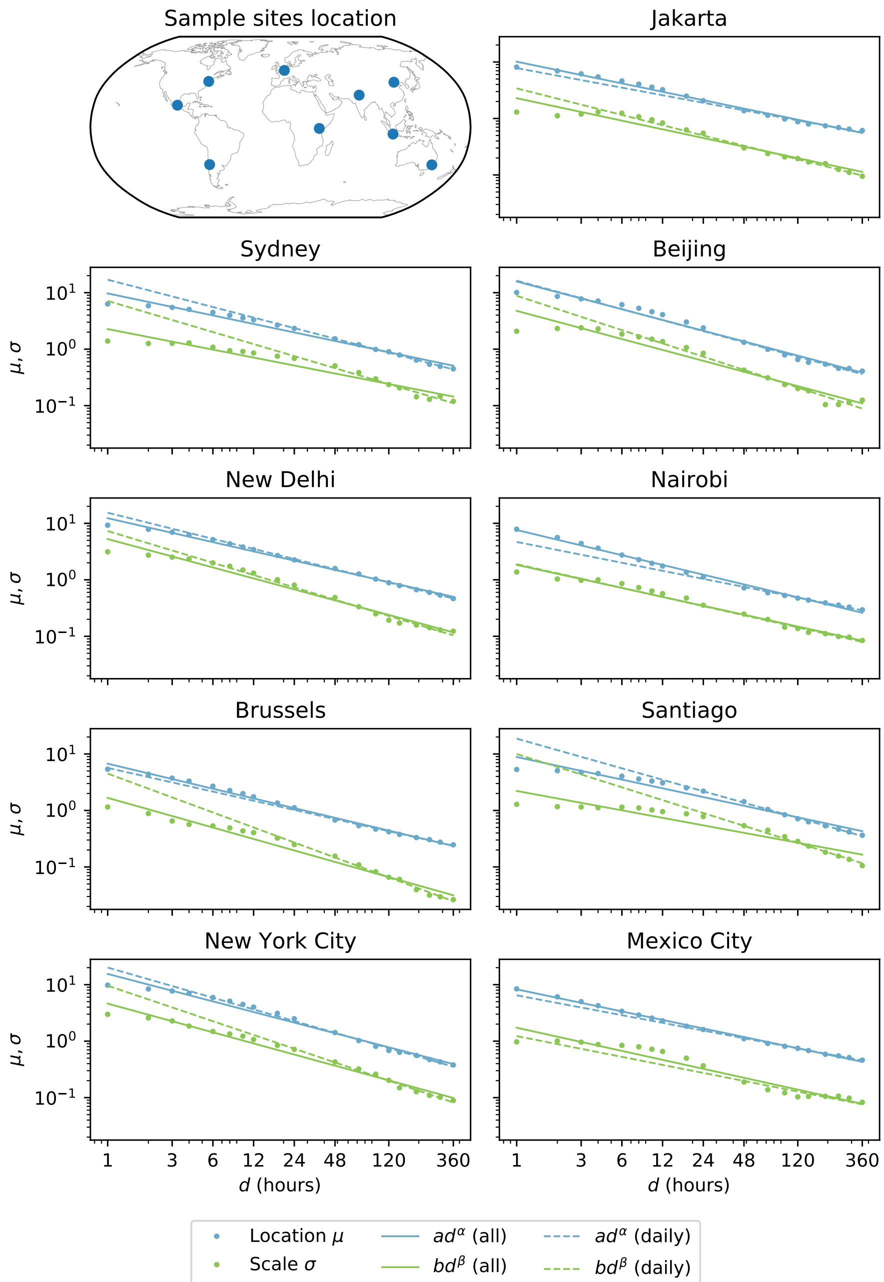

Figure 2: Gumbel parameter scaling at a selection of World cities. The dots represent the Gumbel parameters estimated for a given duration. The the solid regression lines are fitted on all the durations, while the dashed regression lines are fitted on the daily durations and above.

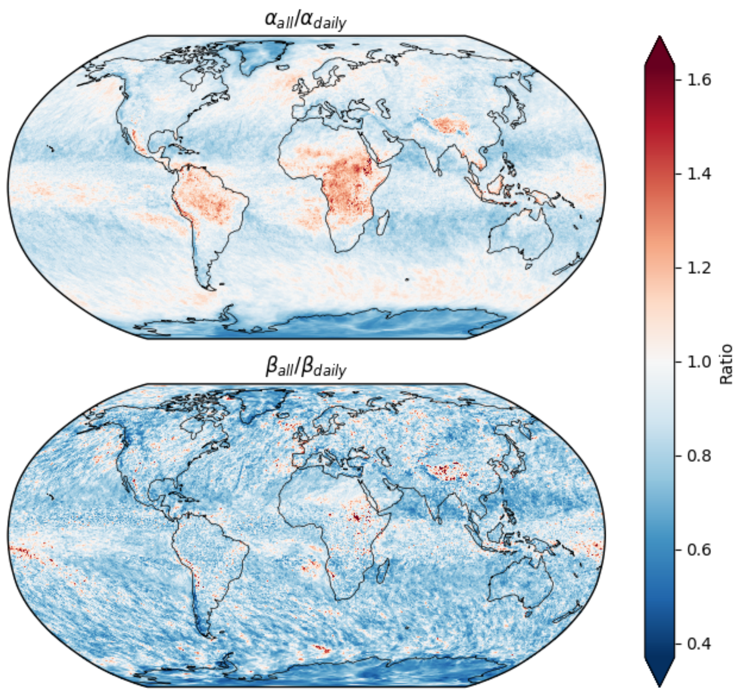

Figure 3: Ratio between the scaling parameters α and β when these are obtained from all the precipitation durations as compared to super-daily durations only (i.e. $\geq 24\,\mathrm{h}$). Ratios below 1 mean that the regression line obtained from daily data has a steeper slope than the one obtained from all the durations, and is therefore more likely to exhibit an apparent overestimation of the parameters at sub-daily durations.

Figure 4 displays the differences between the super-daily regression line and the actual parameters. When using the data from ERA5, the discrepancy between fitted and extrapolated parameters increases most markedly for durations less than 3 and 6 hours respectively for the location and scale values. However, it is noteworthy that this tendency disappears when using data from rain gauges of the Met Office MIDAS database. In the case of MIDAS, the regression line fitted to the daily data is a very good basis for extrapolating the Gumbel parameters of sub-daily rainfall, resulting only in a slight underestimation of the scale parameter σ.

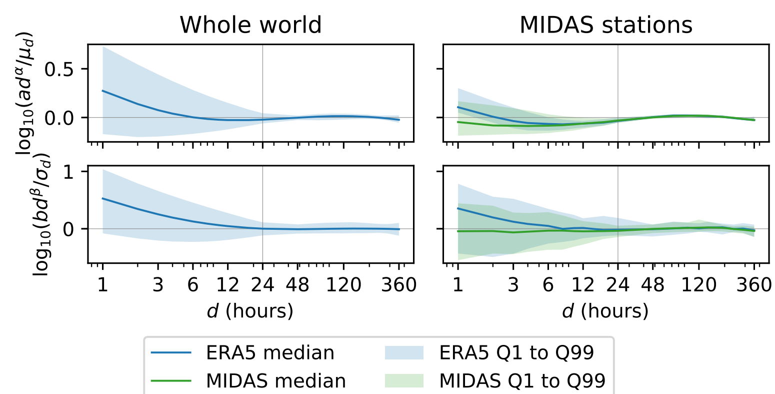

Figure 4: Differences between the Gumbel parameters μ and σ estimated using the scaling parameters a, b, α and β and the actual μ_d and σ_d estimated by fitting the annual maxima. In this case, the regression line is fitted on $d \geq 24\,\mathrm{h}$. The greater the deviation from zero, the less accurate are α and β at estimating μ and σ. Values above zero indicate an overestimation of the Gumbel parameter.

4. Discussion

In this article our preparatory analysis (Section 2.2, Fig. S2) concurs with previous work (Menabde et al., 1999) suggesting that the annual maxima of precipitation intensities are usefully described as following a Gumbel distribution. However, we show this applies on a global scale using the newly-compiled PXR-2 dataset (Section 3.1) (Courty et al., 2018).

PXR provides a useful simplified description of global extreme precipitation. By describing the entire intensity–frequency distribution for a given d with only two parameters (i.e. not mean, median, mode, range etc.), more meaningful inter-comparison between areas is facilitated as it has been in analogous situations in other research fields (e.g. Hillier et al., 2013). The utility of PXR is enhanced by the relative ease with which the Gumbel parameters and their spatial distribution (e.g. Fig. 1) can be interpreted. Higher μ indicates greater typical precipitation intensities (i.e. the entire distribution becomes more intense), whilst higher σ values indicate more extreme events in the 'tail' of the distribution. Thus it is, for example, easy to interpret the apparent tendency towards overestimation of the extrapolation presented in Section 3.3. Additionally, we showed in Section 3.1 that the parameter maps constituting PXR-2 represent qualitatively the expected geographical patterns of extreme precipitations, such as monsoon (e.g. south Asia, Kripalani et al., 2007), mountainous regions (e.g. central Andes, Viale et al., 2011), or desert areas (e.g. Antartica, Vaughan et al., 1999).

In depth, this dataset could have hydrological applications ranging from engineering (e.g. Brown et al., 2013; NYS DoT, 2018) to extreme event studies (e.g. Lumbroso et al., 2011) and more widely, perhaps in respect of landslide triggering (e.g. Postance et al., 2018), flood forecasting (e.g. Slater and Villarini, 2016), or in relation to convection indices (e.g. Kunz et al., 2009). Another possible application is the diagnostics of climate and weather models to assess their capacity to reflect the same scaling as those observed in nature.

The results we present suggest that μ is broadly more robust than σ. Indeed, the estimates of σ reveal more variability than those of σ in both space (Fig. 1), duration (Fig. 2), and the scaling property (Fig. 3 and 4). This higher variability of σ might be explained by the fact that the scale parameter is related to the intensity of less probable events (tail of the Probability Density Function); we employ a relatively short series of annual maxima (18 years) that could miss more extreme events. Indeed, using a longer series of annual maxima is key to improving estimates of GEV parameters (Papalexiou and Koutsoyiannis, 2013), although at the risk of overlooking the non-stationary nature of precipitation distribution (Westra et al., 2014). In addition to using longer record lengths, the size of annual maxima series on which the GEV is fitted could be increased by pooling ensemble members (van den Brink et al., 2005) or nearby data points (Overeem et al., 2008).

The analysis also confirms that the Gumbel parameters μ and σ indeed scale with the duration d (e.g. Menabde et al., 1999; Overeem et al., 2008), and that this relationship applies globally. However, in contrast to previous work there is strong evidence that the two Gumbel parameters scale with different gradients (see Section 3.2). As a caveat, we note that the relationship between the parameters and d may be multi-scale (as denoted by breaks in slope of the log-log plots), and that more sophisticated scaling laws may be specified (Clauset et al., 2009). The assumption of a power-law scaling enables the formulation of a general IDF formula that takes only four parameters to describe extreme precipitation at any d for any given location on Earth. The return period T being equal to $1/(1-F)$, we can express (1) in respect to i and obtain the IDF formula (4).

$$i = \mu_d - \sigma_d \ln\left(-\ln\left(1 - 1/T\right)\right) \tag{4}$$

Substituting μ_d and σ_d with their scaled form (2) we obtain a general IDF formula (5) that takes the parameters a, b, α and β specific to a given geographical location. World maps of these parameters are dubbed the PXR-4 dataset and are freely available to accompany this paper (Courty et al., 2018).

$$i = ad^{\alpha} - bd^{\beta} \ln\left(-\ln\left(1 - 1/T\right)\right) \tag{5}$$

The combination of this general formula and PXR-4 allow the estimation of the intensity of precipitation for any duration and return period, anywhere in the world. In addition to the smaller size of PXR-4 (58 MB vs 237 MB for PXR-2) that facilitates its use in low resources environments, this parsimonious representation allows the estimation of IDF curves for a continuous range of durations rather than discrete d in the case of PXR-2.

In addition to providing sub-daily IDF information in parts of the world where no such data is readily available, PXR-2 also gives an insight about the feasibility of using daily rainfall records from pluviometers to estimate sub-daily IDF. Indeed, daily records are more common than data from automatic sub-daily gauges, and the lack of the latter is a challenge for engineers (e.g. Lumbroso et al., 2011). Naturally, applying the general IDF formula (5) results in Gumbel parameters that are different from those obtained from the annual maxima. Those differences are expectedly larger when looking at the scaling based on super-daily durations only (See Fig. 4). However, the same scaling does work down to a duration of one hour when applied to rain gauges from the MIDAS network in the UK.

We suspect that the scaling differences between ERA5 and the rain gauges could be due to two factors. First, the weather model used to generate ERA5 might underestimate the actual rainfall intensities of events of shorter durations, which are likely to be convective in nature and of limited spatial scale (Prein et al., 2015). Second, ERA5 is a gridded product and is therefore expected to give lower intensities than a gauge product (De Michele et al., 2001). Indeed those differences in scaling might not be due to an inadequacy of the scaling hypothesis, but to an under-reporting of short precipitation events in the ERA5 dataset. Namely, it may not be the regression line that overestimates the parameter for short durations, but the observed parameters being underestimated in the first place.

To illustrate the uncertainty introduced by this general IDF formula we compare the sizing of a culvert in an hypothetical 80 ha catchment in Jakarta with a time of concentration Tc of 2 h. For the ten-year rainfall, the use of the general IDF formula results in an increase in the catchment outflow by 13.9 % compared to the direct use of the fitted Gumbel parameters. This difference however does not induce an increase in the culvert diameter that stays at a standard size of 1 m. For the 100 years rainfall however, using the general IDF formula (5) results in an increase of 20.3 % and 32.8 % over the intensity from

(4) when using the scaling fitted on all the durations and the super-daily only, respectively. Meanwhile the pipe diameter must be increased from 1 m to 1.2 m.

In this case, the scaling yields a more precautionary and potentially costly design. However, as discussed previously, more research is needed to identify whether those differences are the results of an underestimation of short rainfall intensities from ERA5, or an overestimation due to the scaling law. The sizing calculations are detailed in Section S1.1.

These encouraging results highlight the promising applicability of 1) reanalysis data to estimate IDF relationships, and 2) daily rainfall records to estimate sub-daily IDF curves. Our findings may be of great interest for engineers working in data scarce regions and earth scientists interested in extreme precipitation variations. The same analyses could be performed with other reanalysis data and with longer time series to study the stationarity of scaling relationships. Future work might include the fitting of the GEV over longer annual maxima series to obtain more robust parameter estimates, or evaluation of the physical causes of multi-scaling properties, including any upper bounds to parameter estimates at very short (< 3 h) durations.

Acknowledgments

This work is supported by the Natural Environment Research Council (NERC) via grant NE/R014361/1. The results are generated using Copernicus Climate Change Service information 2018. The accompanying PXR-2 and PXR-4 datasets are freely available online (Courty et al., 2018).

The Python programming language was used for the processing and plotting of the data, especially the modules xarray (Hoyer and Hamman, 2017), dask (Rocklin, 2015), pandas (McKinney, 2011), SciPy (Jones et al., 2001), matplotlib (Hunter, 2007) and Cartopy (Met Office, 2010).

Authors contributions

All authors conceived the research idea, contributed to interpreting the results and writing the manuscript. Laurent Courty wrote the software, ran the analysis, and created the figures.

References

Ashouri H, Hsu KL, Sorooshian S, Braithwaite DK, Knapp KR, Cecil LD, Nelson BR, Prat OP. PERSIANN-CDR: Daily Precipitation Climate Data Record from Multisatellite Observations for Hydrological and Climate Studies. Bulletin of the American Meteorological Society 2015;96(1):69–83. URL: http://journals.ametsoc.org/doi/10.1175/BAMS-D-13-00068.1. doi:10.1175/BAMS-D-13-00068.1.

Battaglia P, Chocat B, Blanchard M, Others . La Ville et son assainissement. Certu, 2003.

Beck HE, Pan M, Roy T, Weedon GP, Pappenberger F, van Dijk AIJM, Huffman GJ, Adler RF, Wood EF. Daily evaluation of 26 precipitation datasets using Stage-IV gauge-radar data for the CONUS. Hydrology and Earth System Sciences Discussions 2018;:1–23URL: https://www.hydrol-earth-syst-sci-discuss.net/hess-2018-481/. doi:10.5194/hess-2018-481.

Berne A, Delrieu G, Creutin JD, Obled C. Temporal and spatial resolution of rainfall measurements required for urban hydrology. Journal of Hydrology 2004;299(3-4):166–79. URL: https://www.sciencedirect.com/science/article/pii/S0022169404003634. doi:10.1016/J.JHYDROL.2004.08.002.

Blenkinsop S, Lewis E, Chan SC, Fowler HJ. Quality-control of an hourly rainfall dataset and climatology of extremes for the UK. International Journal of Climatology 2017;37(2):722–40. URL: http://doi.wiley.com/10.1002/joc.4735. doi:10.1002/joc.4735.

Bougadis J, Adamows K. Scaling model of a rainfall intensity-duration-frequency relationship. Hydrological Processes 2006;(20):3747–57. doi:10.1002/hyp.6386.

van den Brink HW, Können GP, Opsteegh JD, van Oldenborgh GJ, Burgers G. Estimating return periods of extreme events from ECMWF seasonal forecast ensembles. International Journal of Climatology 2005;25(10):1345–54. URL: http://doi.wiley.com/10.1002/joc.1155. doi:10.1002/joc.1155.

Brown SA, Schall JD, Morris JL, Doherty CL, Stein SM, Warner JC. Urban Drainage Design Manual. Third edit ed.; volume 2009. National Highway Institute, 2013. URL: http://www.fhwa.dot.gov/engineering/hydraulics/library_arc.cfm?pub_number=22&id=140.

Chow VT. Open channel hydraulics. McGraw-Hill Book Company, Inc; New York, 1959.

Clauset A, Shalizi CR, Newman MEJ. Power-Law Distributions in Empirical Data. SIAM Review 2009;51(4):661–703. URL: http://epubs.siam.org/doi/10.1137/070710111. doi:10.1137/070710111.

Copernicus Climate Change Service . Climate Data Store. 2018. URL: https://cds.climate.copernicus.eu.

Courty LG, Wilby RL, Hillier JK, Slater LJ. Parametrized eXtreme Rainfall. 2018. doi:10.5281/zenodo.1467859.

De Michele C, Kottegoda NT, Rosso R. The derivation of areal reduction factor of storm rainfall from its scaling properties. Water Resources Research 2001;37(12):3247–52. URL: http://doi.wiley.com/10.1029/2001WR000346. doi:10.1029/2001WR000346.

Domínguez R, Carrizosa E, Fuentes GE, Arganis ML, Osnaya J, Galván-Torres AE. Análisis regional para estimar precipitaciones de diseño en la república mexicana. Tecnología y Ciencias del Agua 2018;9(1):05–29. doi:10.24850/j-tyca-2018-01-01.

Fowler HJ, Kilsby CG. A regional frequency analysis of United Kingdom extreme rainfall from 1961 to 2000. International Journal of Climatology 2003;23(11):1313–34. URL: http://doi.wiley.com/10.1002/joc.943. doi:10.1002/joc.943.

Gelaro R, McCarty W, Suárez MJ, Todling R, Molod A, Takacs L, Randles CA, Darmenov A, Bosilovich MG, Reichle R, Wargan K, Coy L, Cullather R, Draper C, Akella S, Buchard V, Conaty A, da Silva AM, Gu W, Kim GK, Koster R, Lucchesi R, Merkova D, Nielsen JE, Partyka G, Pawson S, Putman W, Rienecker M, Schubert SD, Sienkiewicz M, Zhao B, Gelaro R, McCarty W, Suárez MJ, Todling R, Molod A, Takacs L, Randles CA, Darmenov A, Bosilovich MG, Reichle R, Wargan K, Coy L, Cullather R, Draper C, Akella S, Buchard V, Conaty A, Silva AMd, Gu W, Kim GK, Koster R, Lucchesi R, Merkova D, Nielsen JE, Partyka G, Pawson S, Putman W, Rienecker M, Schubert SD, Sienkiewicz M, Zhao B. The Modern-Era Retrospective Analysis for Research and Applications, Version 2 (MERRA-2). Journal of Climate 2017;30(14):5419–54. URL: `http://journals.ametsoc.org/doi/10.1175/JCLI-D-16-0758.1`. doi:`10.1175/JCLI-D-16-0758.1`.

van de Giesen N, Hut R, Selker J. The Trans-African Hydro-Meteorological Observatory (TAHMO). Wiley Interdisciplinary Reviews: Water 2014;1(4):341–8. URL: `http://doi.wiley.com/10.1002/wat2.1034`. doi:`10.1002/wat2.1034`.

Hao Z, AghaKouchak A, Nakhjiri N, Farahmand A. Global integrated drought monitoring and prediction system. Scientific Data 2014;1:140001. URL: `http://www.nature.com/articles/sdata20141`. doi:`10.1038/sdata.2014.1`.

Hersbach H, Dick L. ERA5 reanalysis is in production. ECMWF Newsletter 147 2016;(147):7. URL: `http://www.ecmwf.int/sites/default/files/elibrary/2016/16299-newsletter-no147-spring-2016.pdf`.

Hillier J, Smith M, Clark C, Stokes C, Spagnolo M. Subglacial bedforms reveal an exponential sizefrequency distribution. Geomorphology 2013;190:82–91. URL: `https://www.sciencedirect.com/science/article/pii/S0169555X13001049#!` doi:`10.1016/J.GEOMORPH.2013.02.017`.

Hoyer S, Hamman JJ. xarray: N-D labeled Arrays and Datasets in Python. Journal of Open Research Software 2017;5(1). URL: `http:`

//openresearchsoftware.metajnl.com/articles/10.5334/jors.148/. doi:10.5334/jors.148.

Hunter JD. Matplotlib: A 2D Graphics Environment. Computing in Science & Engineering 2007;9(3):90–5. URL: http://ieeexplore.ieee.org/document/4160265/. doi:10.1109/MCSE.2007.55.

Jones E, Oliphant T, Peterson P, Others . SciPy: Open source scientific tools for Python. 2001. URL: http://www.scipy.org/.

Kripalani RH, Oh JH, Kulkarni A, Sabade SS, Chaudhari HS. South Asian summer monsoon precipitation variability: Coupled climate model simulations and projections under IPCC AR4. Theoretical and Applied Climatology 2007;90(3-4):133–59. URL: http://link.springer.com/10.1007/s00704-006-0282-0. doi:10.1007/s00704-006-0282-0.

Kumari M, Singh CK, Basistha A. Clustering Data and Incorporating Topographical Variables for Improving Spatial Interpolation of Rainfall in Mountainous Region. Water Resources Management 2017;31(1):425–42. URL: http://link.springer.com/10.1007/s11269-016-1534-0. doi:10.1007/s11269-016-1534-0.

Kunz M, Sander J, Kottmeier C. Recent trends of thunderstorm and hailstorm frequency and their relation to atmospheric characteristics in southwest Germany. International Journal of Climatology 2009;29(15):2283–97. URL: http://doi.wiley.com/10.1002/joc.1865. doi:10.1002/joc.1865.

Lumbroso D, Boyce S, Bast H, Walmsley N. The challenges of developing rainfall intensity-duration-frequency curves and national flood hazard maps for the Caribbean. Journal of Flood Risk Management 2011;4(1):42–52. URL: http://doi.wiley.com/10.1111/j.1753-318X.2010.01088.x. doi:10.1111/j.1753-318X.2010.01088.x.

McKinney W. pandas: a Foundational Python Library for Data Analysis and Statistics. In: Proceedings of the 1st Workshop on Python for High-Performance and Scientific Computing. 2011. .

Menabde M, Seed A, Pegram G. A simple scaling model for extreme rainfall. Water Resources Research 1999;35(1):335–9. URL: http://doi.wiley.com/10.1029/1998WR900012. doi:10.1029/1998WR900012.

Met Office . cartopy. 2010. URL: https://scitools.org.uk/cartopy.

Met Office . Met Office Integrated Data Archive System (MIDAS) Land and Marine Surface Stations Data (1853-current). 2012. URL: http://catalogue.ceda.ac.uk/uuid/220a65615218d5c9cc9e4785a3234bd0.

Met Office . UK climate - Extremes. 2018. URL: https://web.archive.org/web/20181206185424/https://www.metoffice.gov.uk/public/weather/climate-extremes/.

NYS DoEC . Guidelines for Design of Dams. Technical Report; New York State Department of Environmental Conservation; 1989.

NYS DoT . Highway drainage. In: Highway Design Manual. New York State Department of Transportation; volume 8; 2018. URL: https://www.dot.ny.gov/divisions/engineering/design/dqab/hdm/chapter-8.

Olauson J. ERA5: The new champion of wind power modelling? Renewable Energy 2018;126:322–31. URL: https://www.sciencedirect.com/science/article/pii/S0960148118303677#fig1. doi:10.1016/J.RENENE.2018.03.056.

Ombadi M, Nguyen P, Sorooshian S, Hsu Kl. Developing Intensity-Duration-Frequency (IDF) Curves from Satellite-based Precipitation: Methodology and Evaluation. Water Resources Research 2018;URL: http://doi.wiley.com/10.1029/2018WR022929. doi:10.1029/2018WR022929.

Overeem A, Buishand A, Holleman I. Rainfall depth-duration-frequency curves and their uncertainties. Journal of Hydrology 2008;348(1-2):124–34. doi:10.1016/j.jhydrol.2007.09.044.

Papalexiou SM, Koutsoyiannis D. Battle of extreme value distributions: A global survey on extreme daily rainfall. Water Resources Research 2013;49(1):187–201. URL: http://doi.wiley.com/10.1029/2012WR012557. doi:10.1029/2012WR012557.

Postance B, Hillier J, Dijkstra T, Dixon N. Comparing threshold definition techniques for rainfall-induced landslides: A national assessment using radar rainfall. Earth Surface Processes and Landforms 2018;43(2):553–60. URL: http://doi.wiley.com/10.1002/esp.4202. doi:10.1002/esp.4202.

Prein AF, Langhans W, Fosser G, Ferrone A, Ban N, Goergen K, Keller M, Tölle M, Gutjahr O, Feser F, Brisson E, Kollet S, Schmidli J, van Lipzig NPM, Leung R. A review on regional convection-permitting climate modeling: Demonstrations, prospects, and challenges. Reviews of Geophysics 2015;53(2):323–61. URL: http://doi.wiley.com/10.1002/2014RG000475. doi:10.1002/2014RG000475.

Rocklin M. Dask: Parallel Computation with Blocked algorithms and Task Scheduling. In: Huff K, Bergstra J, editors. Proceedings of the 14th Python in Science Conference. 2015. p. 130–6.

Roux C, Desbordes M. Rainfall-frequency curves with a recent urban dense rainfall measurement network. Atmospheric Research 1996;42(1-4):163–76. URL: https://www.sciencedirect.com/science/article/pii/0169809595000615. doi:10.1016/0169-8095(95)00061-5.

Slater LJ, Villarini G. Recent trends in U.S. flood risk. Geophysical Research Letters 2016;43. doi:10.1002/2016GL071199.Received.

Staffell I, Pfenninger S. Using bias-corrected reanalysis to simulate current and future wind power output. Energy 2016;114:1224–39. URL: https://www.sciencedirect.com/science/article/pii/S0360544216311811. doi:10.1016/J.ENERGY.2016.08.068.

Sun Q, Miao C, Duan Q, Ashouri H, Sorooshian S, Hsu KL. A Review of Global Precipitation Data Sets: Data Sources, Estimation, and Intercomparisons. Reviews of Geophysics 2018;56(1):79–107. URL: http://doi.wiley.com/10.1002/2017RG000574. doi:10.1002/2017RG000574.

Texas DoT . Hydraulic Design Manual, 2016.

UN DESA . 2018 Revision of World Urbanization Prospects. Technical Report; United Nations; 2018. URL: https://www.un.org/development/desa/publications/2018-revision-of-world-urbanization-prospects.html.

Uppala SM, Kllberg PW, Simmons AJ, Andrae U, Bechtold VDC, Fiorino M, Gibson JK, Haseler J, Hernandez A, Kelly GA, Li X, Onogi K, Saarinen S, Sokka N, Allan RP, Andersson E, Arpe K, Balmaseda MA, Beljaars ACM, Berg LVD, Bidlot J, Bormann N, Caires S, Chevallier F, Dethof A, Dragosavac M, Fisher M, Fuentes M, Hagemann S, Hólm E, Hoskins BJ, Isaksen L, Janssen PAEM, Jenne R, Mcnally AP, Mahfouf JF, Morcrette JJ, Rayner NA, Saunders RW, Simon P, Sterl A, Trenberth KE, Untch A, Vasiljevic D, Viterbo P, Woollen J. The ERA-40 re-analysis. Quarterly Journal of the Royal Meteorological Society 2005;131(612):2961–3012. URL: http://doi.wiley.com/10.1256/qj.04.176. doi:10.1256/qj.04.176.

Vaughan DG, Bamber JL, Giovinetto M, Russell J, Cooper APR, Vaughan DG, Bamber JL, Giovinetto M, Russell J, Cooper APR. Reassessment of Net Surface Mass Balance in Antarctica. Journal of Climate 1999;12(4):933–46. URL: http://journals.ametsoc.org/doi/abs/10.1175/1520-0442%281999%29012%3C0933%3ARONSMB%3E2.0.CO%3B2. doi:10.1175/1520-0442(1999)012<0933:RONSMB>2.0.CO;2.

Veneziano D, Furcolo P. Multifractality of rainfall and scaling of intensity-duration-frequency curves. Water Resources Research 2002;38(12):42–1. URL: http://doi.wiley.com/10.1029/2001WR000372. doi:10.1029/2001WR000372.

Viale M, Nuñez MN, Viale M, Nuñez MN. Climatology of Winter Orographic Precipitation over the Subtropical Central Andes and Associated Synoptic and Regional Characteristics. Journal of Hydrometeorology 2011;12(4):481–507. URL: http://journals.ametsoc.org/doi/abs/10.1175/2010JHM1284.1. doi:10.1175/2010JHM1284.1.

Westra S, Fowler HJ, Evans JP, Alexander LV, Berg P, Johnson F, Kendon EJ, Lenderink G, Roberts NM. Future changes to the intensity and frequency of short-duration extreme rainfall. Reviews of Geophysics 2014;52(3):522–55. URL: http://doi.wiley.com/10.1002/2014RG000464. doi:10.1002/2014RG000464.

Xu W, Zou Y, Zhang G, Linderman M. A comparison among spatial interpolation techniques for daily rainfall data in Sichuan Province, China. International Journal of Climatology 2015;35(10):2898–907. URL: http://doi.wiley.com/10.1002/joc.4180. doi:10.1002/joc.4180.

S1. Supplementary material

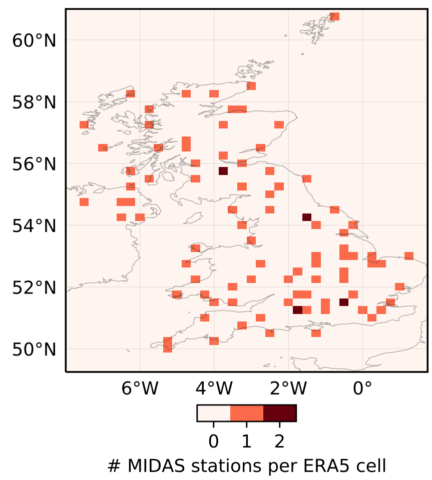

Figure S1: MIDAS rain gauges compared to the ERA5 grid above the British isles. Three stations do not have coordinates and are therefore not represented on this map.

Table S1: Pearson's r^2 for the scaling of the Gumbel parameters location μ and scale σ. For each parameter, the r^2 value is given when looking at all the durations (1 h to 360 h) or only those of 24 h and above. r^2 is computed between $\log(d)$ and $\log(\mu, \sigma)$. The total number of cells is 1 038 240.

	μ_{all}	μ_{daily}	σ_{all}	σ_{daily}
Q1 %	0.907	0.968	0.845	0.870
Q50 %	0.980	0.994	0.983	0.961
Q99 %	0.997	0.9995	0.993	0.999
# cells where $p > 0.01$	5	3	1	142

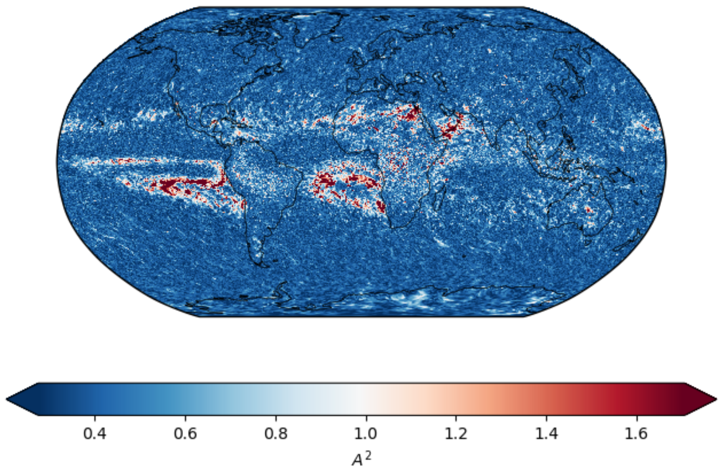

Figure S2: Spatial distribution of the mean of Anderson-Darling A^2 along durations. The centre of the colour bar is the critical value A^2_{crit} at the 1 % significance level. If $A^2 < A^2_{\mathrm{crit}}$, the null hypothesis that the annual maxima follow a Gumbel distribution cannot be rejected.

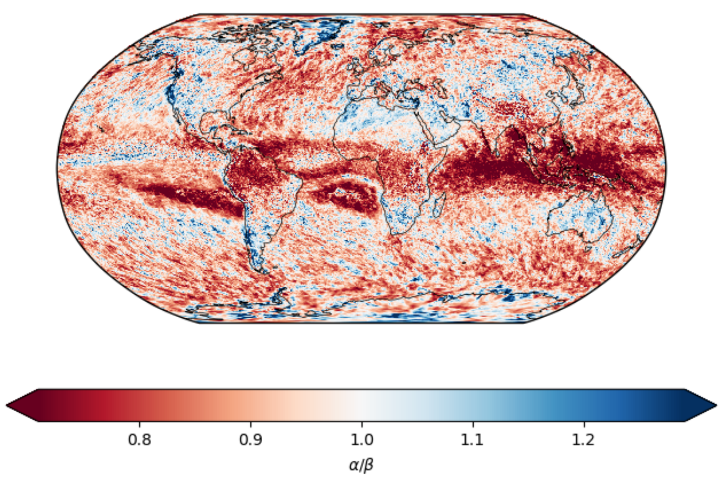

Figure S3: Ratio of the scaling gradients α and β. The more the value deviates from 1, the greater difference between the scaling in duration of the parameters μ and σ

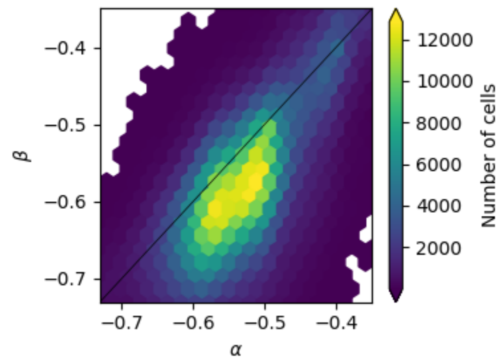

Figure S4: Relation between the scaling gradients α and β of the two Gumbel parameters location μ and scale σ.

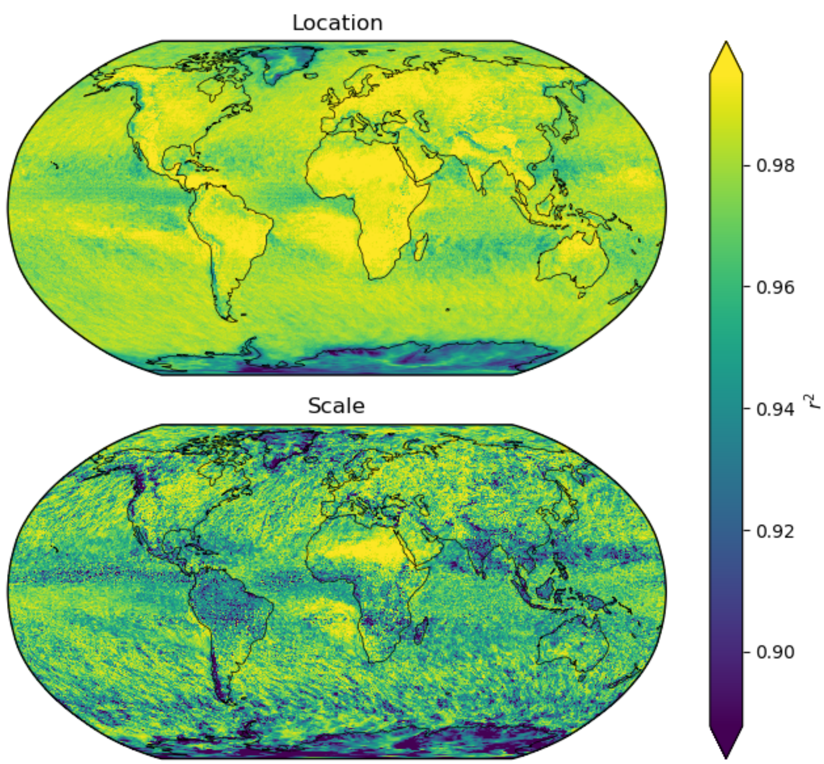

Figure S5: Spatial distribution of the Pearson's r^2 for the Gumbel parameters scaling across all durations. The higher the value, the better the fit of the regression line.

S1.1. Culvert sizing

We consider a catchment with characteristics as described in Table S2. We first estimate the rainfall intensity i by using (4) when using direct parameters or (5) when using scaled parameters.

Then we estimate the flow at the catchment outlet using the rational formula (Texas DoT, 2016)

$$Q = CiA_c/360 \tag{S1}$$

where Q is the peak flow in $\mathrm{m^3\,s^{-1}}$, C the runoff coefficient, i the rainfall intensity and A_c the catchment surface area in ha. In the present case we consider an hypothetical catchment with an area of 80 ha, a runoff coefficient of 0.7 and a time of concentration T_c of 2 h (approximated with a combination of Kirpich and Kerby formulas). We therefore select a 2 h rainfall. The culvert is designed as a circular pipe with a slope S of $5\,\mathrm{mm\,m^{-1}}$. The pipe is sized as the standard diameter able to transit the flow Q when 90 % full. The culvert capacity is estimated with the Gauckler–Manning–Strickler (GMS) formula (Chow, 1959)

$$Q = A_f \frac{1}{n} (\frac{A_f}{P})^{2/3} S^{1/2} \tag{S2}$$

where A_f is the flow area ($\mathrm{m^2}$), P the wetted perimeter (m), and n the Manning's n ($\mathrm{s\,m^{-1/3}}$). We consider that the slope S is parallel to the pipe invert. In the case of a partially filled circular pipe, A_f and P are calculated using (S3)

$$P = \theta\phi \tag{S3a}$$

$$A_f = \frac{1}{8}(\theta - \sin\theta)\phi^2 \tag{S3b}$$

$$\theta = \arccos(1 - \frac{h}{\phi/2}) \tag{S3c}$$

were ϕ is the pipe internal diameter and h the water depth in the pipe.

We do the sizing with two return periods: 10 years and 100 years. We also compare the results obtained with the Gumbel parameters obtained via direct fitting versus those obtained by using the scaling relationship fitted on super-daily durations only and fitted with all the durations.

Table S2: Parameters for culvert sizing at the outlet of an hypothetical catchment in Jakarta. Runoff coefficient C and surface area A_c are hypotheticals. μ_{1h} and σ_{1h} are obtained from direct fitting. μ'_{2h} an σ'_{2h} are obtained by applying the scaling formula.

Parameter	Value	Parameter	Value (all)	Value (daily)
A_c	80 ha	a	10.116	7.807
C	0.7	b	2.286	3.415
d	2 h	α	−0.494	−0.445
T	10 years	β	−0.510	−0.604
μ_{2h}	6.967	μ'_{2h}	7.183	5.735
σ_{2h}	1.117	σ'_{2h}	1.605	2.247

Table S3: Impact of the scaling hypothesis on the sizing of a circular culvert on an hypothetical catchment in Jakarta. Details about the calculation are given in Section S1.1.

Parameter	μ_d, σ_d	Scaling all	Scaling daily
T10 Rainfall ($\mathrm{mm\,h^{-1}}$)	9.5	10.8	10.8
T10 Outflow ($\mathrm{m^3\,s^{-1}}$)	1.5	1.7	1.7
T10 Pipe diameter (m)	1.0	1.0	1.0
T100 Rainfall ($\mathrm{mm\,h^{-1}}$)	12.1	14.6	16.1
T100 Outflow ($\mathrm{m^3\,s^{-1}}$)	1.9	2.3	2.5
T100 Pipe diameter (m)	1.0	1.2	1.2